

The Formation of Stellar Clusters in Turbulent Molecular Clouds: Effects of the Equation of State

Yuxing Li^{1,2}, Ralf S. Klessen³ and Mordecai-Mark Mac Low^{1,2}

¹*Department of Astronomy, Columbia University, New York, NY 10027, USA*

²*Department of Astrophysics, American Museum of Natural History, 79th Street at Central Park West, New York, NY 10024-5192, USA*

³*Astrophysikalisches Institut Potsdam, An der Sternwarte 16, D-14482 Potsdam, Germany*

yxli@astro.columbia.edu, rklessen@aip.de, mordecai@amnh.org

ABSTRACT

We study the effect of varying the equation of state on the formation of stellar clusters in turbulent molecular clouds, using three-dimensional, smoothed particle hydrodynamics simulations. Our results show that the equation of state helps determine how strongly self-gravitating gas fragments. The degree of fragmentation decreases with increasing polytropic exponent γ in the range $0.2 < \gamma < 1.4$, although the total amount of mass accreted onto collapsed fragments appears to remain roughly constant through that range. Low values of γ are expected to lead to the formation of dense clusters of low-mass stars, while $\gamma > 1$ probably results in the formation of isolated and massive stars. Fragmentation and collapse ceases entirely for $\gamma > 1.4$ as expected from analytic arguments. The mass spectrum of overdense gas clumps is roughly log-normal for *non*-self-gravitating turbulent gas, but changes to a power-law under the action of gravity. The spectrum of collapsed cores, on the other hand, remains log-normal for $\gamma \leq 1$, but flattens markedly for $\gamma > 1$. The density PDFs approach log-normal, with widths that decrease with increasing γ . Primordial gas may have effective $\gamma > 1$, in which case these results could help explain why models of the formation of the first stars tend to produce isolated, massive objects.

Subject headings: ISM: clouds — ISM: hydrodynamics — stars: formation — equation of state — turbulence

1. INTRODUCTION

Stars form alone and in groups, associations, and clusters (see Pudritz 2002 and Ward-Thompson 2002 for recent reviews). Yet the origin of this diversity in the process of star formation remains poorly understood. Recent work suggests that stars form by gravitational collapse of shock-compressed density fluctuations generated by the supersonic turbulence generally observed in molecular clouds (e.g. Elmegreen 1993; Padoan & Nordlund 1999; Klessen, Heitsch, & Mac Low 2000; Ostriker, Stone, & Gammie 2001; see Mac Low & Klessen 2003 for a recent review). If so, then star formation is controlled by turbulent fragmentation and dynamical collapse of individual, Jeans-unstable, protostellar clumps.

Fragmentation of gas clouds has been studied for more than a century, yet the process remains poorly understood. There have been analytical models (Jeans 1902; Low & Lynden-Bell 1976), and numerical investigations of the effects of various physical processes on the collapse, such as geometry and rotation of the clouds (see Bonnell & Bastien 1993 for a review), and magnetic fields (Galli et al. 2001). Recently, the effects of turbulence have been studied extensively in a series of three-dimensional simulations using both grid-based, Eulerian and particle-based, Lagrangian hydrodynamics (Klessen, Burkert, & Bate 1998; Klessen & Burkert 2000, hereafter Paper I; Klessen, Heitsch, & Mac Low 2000, Paper II; Heitsch, Mac Low, & Klessen 2001, Paper III; and Klessen 2001, Paper IV). These papers show that turbulence strongly influences the fragmentation of molecular clouds. Fast, clustered collapse and star formation occurs in regions with turbulence insufficient to support against gravitational collapse, while slow, scattered star formation results from strong turbulent support. However, these results are based on isothermal models with polytropic exponent $\gamma = 1$ only. The role of the equation of state (EOS), which is essential in understanding the physical structure and stability of the turbulent clouds, remained unexplored.

The balance of heating and cooling in a molecular cloud can be approximately described by a polytropic EOS

$$P = K\rho^\gamma, \tag{1}$$

where K is a constant, and P, ρ and γ are thermal pressure, gas density and polytropic exponent, respectively. The density structure generated by supersonic motions in highly compressible turbulence depends on the EOS. The stiffness of the EOS can largely control the density probability distribution function (PDF) in strongly compressible turbulence (Scalo 1998; Passot & Vázquez-Semadeni 1998; Vázquez-Semadeni & Garcia 2001). In particular, one-dimensional simulations by Passot & Vázquez-Semadeni (1998) show the shape of the density PDF varying with γ . They found that the PDF is log-normal when $\gamma = 1$ (isothermal), and develops a power-law tail for $\gamma \neq 1$. Spaans & Silk (2000) showed that radiatively cooling gas can be described by a piecewise polytropic EOS, in which the poly-

tropic exponent γ changes with gas density ρ . They conducted a detailed analysis including chemistry, thermal balance and radiative transfer, and found that in the interstellar medium the effective polytropic exponent γ has a range of $0.2 < \gamma < 1.4$. They further predicted that the initial mass function (IMF) of protostellar cores would vary with γ , yielding a peaked IMF for $\gamma > 1$ and a power-law function for $\gamma < 1$.

In this paper, we perform three-dimensional simulations of self-gravitating, supersonic turbulence over the range of γ identified by Spaans & Silk (2000) to investigate the effect of varying the EOS on the dynamical evolution and fragmentation behavior of turbulent clouds and the subsequent formation of protostellar clusters. To quantify the dependency on γ , we consider a true polytropic EOS, with γ being strictly constant in each simulation regardless of the density, rather than the piecewise polytrope used by Spaans & Silk (2000) and earlier workers.

In §2 we describe our computational methods; in §3 we give results on fragmentation, the resulting mass distribution of protostellar cores, and the gas density PDF; and in §4 we conclude and speculate about the implications of our work for the formation of star clusters and primordial star formation.

2. METHODS

In analytical work on the stability of a self-gravitating, isothermal medium, Jeans (1902) derived a relation between the oscillation frequency ω and the wavenumber k of small perturbations,

$$\omega^2 - c_s^2 k^2 + 4\pi G \rho = 0 \quad (2)$$

where c_s is the isothermal sound speed, G the gravitational constant, and ρ is the gas density. The medium is unstable to fragmentation at all wavelengths greater than a critical length $\lambda_J = 2\pi/k_J$, or equivalently all masses exceeding the Jeans mass,

$$M_J = \rho \lambda_J^3 = \left(\frac{\pi}{G}\right)^{3/2} \rho^{-1/2} c_s^3 \quad (3)$$

will collapse under their own weight. Note that we use a cubic definition of M_J .

In a polytropic cloud with EOS given by equation 1, the sound speed is

$$c_s = \left(\frac{dP}{d\rho}\right)^{1/2} = (K\gamma)^{1/2} \rho^{(\gamma-1)/2}, \quad (4)$$

so the Jeans mass will be given as a function of γ and ρ ,

$$M_J = \left(\frac{K\pi}{G}\right)^{3/2} \gamma^{3/2} \rho^{\frac{3}{2}(\gamma-\frac{4}{3})}. \quad (5)$$

The specific internal energy is $u = K\rho^{\gamma-1}/(\gamma_{ad} - 1)$, where γ_{ad} is the adiabatic index, with $\gamma_{ad} = 5/3$ for ideal gas. For isothermal gas, $\gamma = 1$, and $K = c_s^2$.

We carry out simulations to determine when and how fragmentation occurs. We use a smoothed particle hydrodynamics (SPH) code (Benz 1990) in order to resolve several orders of magnitude in density during the collapse of shock-compressed regions. Our version of the code includes periodic boundary conditions (Klessen 1997) and can replace high-density cores with sink particles (Bate, Bonnell, & Price 1995). Sink particles accrete surrounding gas particles while conserving mass and momentum, but they only interact gravitationally. They prevent time step from becoming prohibitively short in very dense regions. This allows us to follow the dynamical evolution of the system over many free-fall times.

We set up a periodic cube with side length $L = 2$ and total mass of unity such that initial density $\rho_0 = 0.125$, and sound speed $c_s = 0.1$. The treatment of the polytropic EOS follows Bonnell & Bastien (1991), where we set $K = (R_g/\mu)T_0\rho_0^{1-\gamma}$. We choose values consistent with the sound speed of $R_g = 2/3$, $\mu = 1$, and $T_0 = 0.015$ for the gas constant, mean molecular weight, and initial temperature of the cloud. Uniform turbulence is driven with the method described by Mac Low et al. (1998) and Mac Low (1999), adding energy over a small range of wavenumbers k . Driving in two wavenumber ranges is considered here, $1 \leq k \leq 2$ and $7 \leq k \leq 8$, corresponding to models *B1h* and *B3* in Paper II. In each case, the driving strength is chosen to ensure the same rms velocity despite the different driving wavenumbers, so that the average turbulent Jeans mass $\langle M_J \rangle_{turb} = 3.2$ and Jeans Number $N_J = 64$, are the same. In a self-gravitating medium, the maximum resolvable density is determined by the requirement that the local thermal Jeans mass be resolved by the SPH kernel (Bate & Burkert 1997); our models all have the same resolution limit.

The models presented here are computed in normalized units. If scaled to mean densities of $n(\text{H}_2) \approx 10^2 \text{cm}^{-3}$, and a temperature of 11.4K (i.e. an isothermal sound speed $c_s = 0.2 \text{km s}^{-1}$), values appropriate for a dark cloud like Taurus (Hartmann 1998), then our simulation cube holds a mass of $M \approx 4 \times 10^3 M_\odot$ and has a size of $L \approx 9 \text{pc}$. For details on the scaling relations, see Paper II.

We computed models with $0.2 \leq \gamma \leq 1.4$, covering the range suggested for interstellar gas by Spaans & Silk (2000). We vary γ in steps of 0.1 in otherwise identical simulations for both driving wavenumbers. Each simulation starts with a uniform density $\rho_0 = 0.125$. Driving begins immediately, while self-gravity is turned on at $t=2.0$, after the turbulence is fully established (see Paper II). Our models use 200 000 particles. Twenty-six simulations were performed simultaneously using a serial version of the code on single 1 GHz Pentium III processors of the Parallel Computing Facility of the American Museum of Natural History (AMNH). Each computation took about 6 months.

3. RESULTS

3.1. Turbulent Fragmentation

Figure 1 and Figure 2 show the density distribution of the gas. To make the figures, a 256^3 grid was filled with densities properly computed from the SPH kernel, and the result is displayed in three-dimensional projection (*top row*) and in a slice through maximum density one free-fall time after self-gravity is turned on for selected γ and both driving wavenumbers. As found in previous studies (e.g. Mac Low 1999), the driving wavenumber strongly influences the density distribution. Driving with $k = 1-2$ produces strong filamentary structure, while the density distribution for $k = 7-8$ remains more uniform at large scale.

We find that the value of γ is as important as the driving in determining collapse behavior. As γ increases, the number of collapsed cores replaced by sink particles decreases, and the cores cluster less. For the same γ , driving with $k = 1-2$ produces both far more, and more clustered dense cores than driving with $k = 7-8$. The dense cores tend to collapse predominantly in filaments or at intersections of filaments. At $\gamma \geq 1.1$, no fragmentation occurs by the time shown for driving with $k = 7-8$.

The isothermal case, $\gamma = 1.0$, agrees well with previous results in Papers II and III. Our current investigation agrees with the results in Paper I–III, that collapse tends to form clusters with high efficiency in regions with weak turbulence, while in regions with strong turbulence, sparse, slow collapse occurs. We now add the additional criterion that collapse and fragmentation depends strongly on γ .

In regions with $\gamma < 1$, fragmentation occurs earlier and more frequently, while in regions where $\gamma > 1$, fragmentation is retarded and less frequent.

Figure 3 compares the number of collapsed cores at different γ for models with different driving wavenumbers. The rate at which new protostellar cores form differs for different γ . Models with low γ form cores quickly, while models with large γ form new cores more rarely. Again we see more cores for driving with $k = 1-2$ than for $k = 7-8$.

Rouleau & Bastien (1990) found an empirical scaling relation $J_c \propto \gamma^2$ of the critical Jeans number $J_c = M/M_J$ for collapse for elongated clouds. The Jeans number should be related to the number of fragments. However, with higher resolution and more statistics for a wide range of γ in our simulations, we find something more like the inverse, but strongly dependent on the details of the driving. Fig 4 shows the relation between the value of γ and the number of fragments at one free-fall time. The number of fragments drops quickly as γ increases for driving with $k = 1-2$, and more slowly for driving with $k = 7-8$, which produces fewer fragments to begin with.

Figure 5 shows the accretion histories (the time evolution of the combined mass fraction of all protostellar cores) for all the individual γ cases and for both driving wavelengths. Note that much less mass is accreted when driving with $k = 7-8$. We focus on the $k = 1-2$ model. The lower γ is, the earlier fragmentation occurs and the larger the number of fragments that form. It also takes longer for the clouds with high γ to fragment. The slope of the accretion curves are roughly the same, but the number of sinks is very different for different γ at the same time, which suggests that the average core mass is different for different γ . A low- γ environment produces a large number of collapsed cores of relatively low mass, while $\gamma > 1$ results in the formation of considerably fewer, but more massive, cores. Since the overall mass growth rate of collapsing cores is closely related to the expected star formation rate, our result suggests that the overall star formation rate is higher in low- γ clouds than in high- γ clouds. It remains unclear what the final amount of mass in stars will be, as higher mass stars may drive surrounding gas away more quickly (see also Vázquez-Semadeni, Ballesteros-Paredes, & Klessen 2003).

We do not find any signs of collapse in the model with $\gamma = 1.4$ even after several free-fall times. This can be explained with a Jeans mass analysis giving the critical condition for gravitational collapse. From Equation [5], we have

$$\frac{\partial M_J}{\partial \rho} \propto \frac{3\gamma - 4}{2} \rho^{(3\gamma-6)/2}. \quad (6)$$

This implies that for $\gamma < 4/3$ the Jeans mass M_J decreases as density increases during collapse; for $\gamma = 4/3$, M_J remains constant; while if $\gamma > 4/3$, then M_J *increases* with density. Thus, any collapse will choke itself off when $\gamma > 4/3$, as found in our numerical results.

Fragmentation is a complex process depending on the local conditions in the cloud, so the above analysis for an isolated spherical perturbation is an approximation. Indeed, fragmentation already ceases for $\gamma > 1.1$ in the model driven with $k = 7 - 8$, suggesting the importance of the details of the turbulence in determining collapse behavior.

3.2. Mass Spectrum

Observations suggest that the mass distribution of gas clumps in molecular clouds follows a power law, $dN/dM = M^\nu$, with typical values of the exponent being $\nu \approx -1.5$ (e.g. Williams, Blitz, & McKee 2000). Salpeter (1955) derived a power law for the high mass stellar IMF in the same notation with $\nu = -2.35$ (see also Scalo 1998; Kroupa 2002).

We measure clump-mass spectra in our models using a clump-finding algorithm similar

to the one described by Williams, De Geus, & Blitz (1994) but working on all three spatial coordinates and adapted to make use of the SPH kernel smoothing procedure (for details see Appendix A in Paper I). Figure 6 shows the spectra of gas clumps and collapsed cores for models with different values of γ , driven with $k = 1-2$. Three different evolutionary phases are shown: after turbulence has been fully established, but before self-gravity has been turned on, at $t = 2$; and when the fraction of mass accumulated in collapsed cores (sink particles) has reached $M_* \approx 20\%$ and 40% .

The mass distribution of both clumps and collapsed cores changes with γ , with the effect being most pronounced for the cores. In low- γ models, the core mass spectrum at the high-mass end is roughly log-normal. As γ increases, fewer but more massive cores emerge. When $\gamma > 1.0$, the distribution is dominated by a few high mass cores, and the spectrum tends to flatten out. It is no longer fit by either a log-normal or a power-law. The clump mass spectra, on the other hand, do show power-law behavior on the high mass side, even for $\gamma > 1.0$.

Our results suggest that massive stars can form in small groups or even in isolation in gas with $\gamma > 1.0$. Spaans & Silk (2000) suggested that a stiff EOS with $\gamma > 1.0$ should lead to a peaked IMF, biased toward massive stars, while an EOS with $\gamma < 1.0$ results in a power-law IMF, in general agreement with our simulations.

3.3. Density Probability Distribution Function

Figure 7 shows mass and volume weighted PDFs of gas density p_m and p_v before self-gravity has been turned on for selected values of γ and both driving wavenumbers. We also show Gaussian fits to the PDFs together with their error $\epsilon = \sum |p - p_{fit}|/p$, summed over all points above 10% of the peak values.

The mass-weighted density PDF $p_m(\rho)$ is calculated directly from the local density associated with each SPH particle, as described by Klessen (2000). The volume-weighted density PDF $p_v(\rho)$ is calculated on a cubic grid derived from the SPH density field by taking a cube of 256^3 cells and using the SPH kernel smoothing procedure to find the density at the center of each cell. Both $p_m(\rho)$ and $p_v(\rho)$ are normalized so that $\int_{-\infty}^{\infty} p_m(\rho)d\rho = \int_{-\infty}^{\infty} p_v(\rho)d\rho = 1$.

The density behind shocks in supersonic turbulence depends on the compressibility of the gas,

$$d\rho \propto \frac{1}{\gamma} P^{\frac{1}{\gamma}-1} dP, \quad (7)$$

So turbulent density fluctuations should increase as γ decreases. Indeed, we see that in Figure 7, the width of p_m and p_v increases as γ decreases.

In models driven with wavenumber $k = 7 - 8$, there are super-Gaussian tails in the low-density end in the volume-weighted PDFs for all γ and in the mass-weighted PDF for $\gamma = 0.2$. One-dimensional simulations by Passot & Vázquez-Semadeni (1998) showed that the volume-weighted density PDF of supersonic turbulent gas displays a power-law tail at high densities for $0 < \gamma < 1$, becomes log-normal for $\gamma = 1$ (isothermal), and develops a power-law tail at low density for $\gamma > 1$, which is only in partial agreement with our results. The discrepancy may be due to the low resolution in low-density regions in our simulations, the difference between one- and three-dimensional simulations, or different driving.

A full investigation of the density PDFs under various conditions, with different codes, different dimensions (three-dimensional vs. one-dimensional), different resolution, different turbulence driving, different initial Mach number, and with and without magnetic field is beyond the scope of this paper; these issues will be addressed elsewhere.

3.3.1. Comparison Between Mass and Volume Weighting

In order to compare the mass and volume weighted PDFs, we will find it useful to define $s = \ln(\rho/\rho_0)$; the mass and volume weighted PDFs of s are then $p_m(s)$ and $p_v(s)$, respectively. We can relate $p(s)$ to $p(\rho)$ if we remember that for any monotonic function $y(x)$, it can be shown that the PDF $|p(y)dy| = |p(x)dx|$. Therefore,

$$p_m(\rho) = p_m(s) \frac{ds}{d\rho} = \frac{p_m(s)}{\rho}, \quad (8)$$

and

$$p_v(\rho) = p_v(s) \frac{ds}{d\rho} = \frac{p_v(s)}{\rho}. \quad (9)$$

Since $p_m(\rho) \propto dM/d\rho$, and $p_v(\rho) \propto dV/d\rho$ (Ostriker, Stone, & Gammie 2001), it follows that

$$p_m(\rho) \propto \frac{dM}{dV} \frac{dV}{d\rho} \propto \rho p_v(\rho). \quad (10)$$

Then we can relate $p_m(s)$ to $p_v(s)$

$$p_m(s) = \rho p_m(\rho) = C \rho^2 p_v(\rho) = C e^s p_v(s). \quad (11)$$

where C is a normalization constant.

If $p_v(s)$ follows a normal distribution,

$$p_v(s) = \frac{1}{\sqrt{2\pi}\sigma} \exp\left(-\frac{(s - s_v)^2}{2\sigma^2}\right), \quad (12)$$

where s_v is the average (in volume) value of s , and σ is the dispersion, then

$$p_m(s) = \frac{C}{\sqrt{2\pi}\sigma} \exp\left(-\frac{s_v^2 - (s_v + \sigma^2)^2}{2\sigma^2}\right) \exp\left(-\frac{[s - (s_v + \sigma^2)]^2}{2\sigma^2}\right). \quad (13)$$

Since $\int_{-\infty}^{\infty} p_m(s) ds = 1$, the normalization

$$C = \exp\left(\frac{s_v^2 - (s_v + \sigma^2)^2}{2\sigma^2}\right). \quad (14)$$

Equation 13 can thus be rewritten as:

$$p_m(s) = \frac{1}{\sqrt{2\pi}\sigma} \exp\left(-\frac{(s - s_m)^2}{2\sigma^2}\right). \quad (15)$$

where $s_m = s_v + \sigma^2$. This is also a normal distribution, with the same dispersion σ as that of p_v but shifted average value s_m . Using the volume PDF normalization $\int \rho \cdot p_v(s) ds = \int e^s p_v(s) ds = 1$, it can be seen

$$s_m = -s_v = \frac{\sigma^2}{2}. \quad (16)$$

as noted, for example, by Ostriker, Stone, & Gammie (2001). This holds only if the density PDF is log-normal. (Note that in this case $C = 1$.)

This derivation gives several properties of the density PDFs p_m and p_v . If one of them is log-normal, so is the other; and if they are log-normal, the width σ of both profiles should be equal (Eqs. [12] and [15]), and the peaks of the PDFs $p_m(s)$ and $p_v(s)$ should lie symmetrically around zero (Eq. [16]).

In Figure 7 the volume-weighted PDFs lie to the left of the mass-weighted PDFs, with $s_m \approx -s_v$, as predicted. The decent Gaussian fits to the peaks of the PDFs show that the assumption of log-normal behavior is not bad. Three-dimensional grid-based simulations of decaying turbulence by Ostriker, Stone, & Gammie (2001) show similar Gaussian PDFs.

A detailed examination of the moments of the density PDFs, shown in Fig 8, shows that these PDFs are, in fact, not perfect log-normals. The first moment (mean) shows that p_m and p_v of models with both driving wavenumbers $k = 1 - 2$ and $k = 7 - 8$ are not exactly symmetrically distributed. This could be due to turbulent intermittency in our small boxes producing deviations from a purely Gaussian distribution. The Gaussian behavior expected

from a well sampled distribution is more visible in models driven with $k = 7 - 8$ compared to $k = 1 - 2$. In fact, p_m and p_v of $k = 7 - 8$ are more equal in width, as seen from the second moment (variance). This is a sign of better sampling – more modes contribute to the overall velocity field, thus the central limit theorem is more appropriately applied to the $k = 7 - 8$ than to the $k = 1 - 2$ case (Klessen 2000).

3.3.2. *Effect of Self-Gravity*

Figure 9 shows the evolution of the mass-weighted gas density PDF p_m of the model driven with $k = 1 - 2$ for different values of γ . The same three evolutionary phases as defined in §3.2 are shown: the initial distribution, and times at which dense cores have accreted $M_* \approx 20\%$ and $M_* \approx 40\%$ of the mass. These PDFs do not include gas accreted into the cores. We again show the best-fit Gaussian for the part of each PDF above 10% of peak.

During the dynamical evolution, the PDFs in the non-isothermal cases develop pronounced positive deviations from the the Gaussian fit, while the PDF in the isothermal case remains well fit by a Gaussian (of increasing width), consistent with the results in Klessen (2000). The high-density tails gradually diminish as γ increases from 0.2 to 1.0, vanishing almost entirely at $\gamma = 1.0$. At $\gamma > 1.0$, though, the tails develop again and get stronger as γ continues to increase. We do not fully understand why the tails only appear in non-isothermal cases.

The first four moments of the density PDFs for each of the three evolutionary phases discussed previously are shown in Figure 10. We can see that the moments vary as collapse proceeds, demonstrating that self-gravity plays an important role in shaping the density PDF.

The plot of the skewness shows that the PDFs of turbulence without self-gravity are always skewed to low densities, regardless of γ . Shock compression comes at a cost: the gas swept up in shock fronts has to come from somewhere, and those regions now contain only low-density gas. As the filling factor of shocks is low (Smith, Mac Low, & Heitsch 2000) most of the volume is occupied by these low-density regions resulting in PDFs with negative skewness. The situation changes, however, when self-gravity comes into play. Gravitational contraction produces high densities in addition to the turbulent shock compression, the PDF's in the later stages of evolution are thus strongly biased towards high-density gas and the skewness becomes positive.

4. SUMMARY AND DISCUSSION

We have investigated the effect of varying the equation of state (EOS) on the formation of stellar clusters in turbulent molecular clouds using a set of three-dimensional numerical simulations. Our results show that the EOS plays an important role in the fragmentation of the clouds, the determination of the initial mass function (IMF) of the protostellar cores, and the shape of the gas density PDFs.

The ability of interstellar gas clouds to fragment under the action of self-gravity *decreases* with *increasing* polytropic exponent γ in the range $0.2 < \gamma < 1.4$ relevant for Galactic molecular clouds. The total amount of mass in collapsed cores, however, appears to remain roughly constant through that range. At least half of this material is expected to accrete onto the protostellar system at the center of each collapsing core (e.g. Klessen 2001). Small values of γ thus lead to the formation of dense clusters of predominantly low-mass stars, while $\gamma > 1$ results in the formation of isolated and massive stars. Fragmentation and collapse ceases entirely for $\gamma > 1.4$ as expected from analytic arguments.

The mass spectra of both clumps and collapsed cores change with γ , with that effect being most pronounced for the cores. For $\gamma \leq 1.0$, their mass spectrum appears roughly log-normal. As γ increases, fewer but more massive objects emerge. When $\gamma > 1.0$, the distribution is dominated by high mass objects only, and the spectrum tends to flatten out. It is fit by neither a log-normal nor a power-law. The clump mass spectra, on the other hand, do show power-law behavior at the high mass end for all γ .

The density PDF changes with γ as well. The width of the profile decreases as γ increases, as expected from analytic arguments about shock compression. Both mass- and volume-weighted PDFs show imperfect log-normal distributions. Self-gravity helps shape the PDF. During dynamical collapse, the PDF develops a high-density tail, which is the imprint of local collapse of high density regions.

In a polytropic gas cloud, any temperature fluctuation corresponds to a density fluctuation, $\Delta \log_{10}(T) \simeq \Delta \log_{10}(\rho)(1-\gamma) - 0.6$. We note that from the gas density PDFs in Figure 7, the maximum width of the profiles is about 12, which corresponds to $\Delta \log_{10}(\rho) \simeq 5$. So for the extreme case $\gamma = 0.2$, $\Delta \log_{10}(T) \simeq 3.5$. For a cloud with an average temperature of about 10 K the maximum temperature of the low-density gas therefore could reach values up to 10^4 K, if γ is extremely low. This still falls in the temperature range observed in star forming regions.

The principal motivation of this paper is to investigate how the fragmentation behavior of a turbulent cloud and the subsequent formation of stars are affected by physical state of the cloud, as described by the EOS. Since γ reflects the balance between heating and

cooling, γ is expected to be low in regions of strong cooling, while γ may be large where the cooling mechanism is insufficient (Spaans & Silk 2000). Unfortunately, the true chemical state and composition of interstellar gas is difficult to assess, so exact values of γ are difficult to estimate observationally.

The possibility that isolated, massive stars form when $\gamma > 1$ is of interest, not only because ionizing radiation, stellar winds, and supernovae from massive stars play an important role in the interstellar medium, but also because massive stars are rarely observed in isolation. Rather, they are usually found as members of rich stellar clusters. Recently, however, Lamers et al. (2002) has reported observations of massive stars found in isolation or associated only with very small groups of lower-mass stars in the bulge of M51. Massey (2002) also reported finding apparently isolated, massive, field stars in both the Large and Small Magellanic Clouds. Our simulations suggest that molecular cloud regions forming isolated, high-mass stars have $\gamma > 1$. In this case turbulent cloud fragmentation tends to produce isolated, massive collapsing cores that will feed onto isolated high-mass stars. Yorke & Sonnhalter (2002) demonstrated that high-mass stars can form in collapsing gas clumps via disk accretion very much the same way as low mass stars are believed to do. There is thus no need for a dense cluster environment where high-mass stars could build up by collisions of lower-mass stars (as suggested by Bonnell, Bate, & Zinnecker 1998).

A theory of galactic-scale star formation partially based on the universality of log-normal density PDFs has been proposed by Elmegreen (2002). Our results do show a log-normal form at least for the peak of the PDFs, containing most of the gas. However, the dispersion of the PDF varies substantially as the EOS changes (Fig. 8), so that the fraction of gas available for star formation would depend significantly on the EOS in such a theory. This raises the question of how it could still be able to explain a global Schmidt Law across many different galaxies with different metallicities, radiation fields, interstellar pressures, and so forth.

High resolution simulations by Abel, Bryan, & Norman (2000, 2002) of the formation of the first star suggest that fragmentation during the collapse of metal-free pregalactic halos is rather inefficient, resulting in the formation of single, massive stars rather than clusters of lower-mass objects. In the absence of metals, inefficient cooling may result in high γ , perhaps helping to explain these results.

We do note, however, that simulations by Bromm, Coppi, & Larson (1999, 2002) show greater multiplicity. They use similar chemistry, but examine more massive, more isolated halos, with substantially larger limiting mass resolution. The EOS will have less effect on these larger scales, which are more dominated by gravity. If the metal-free gas indeed shows a high effective γ , our models would suggest that their collapsing regions will show little

further fragmentation if followed down to stellar mass scales.

We thank M. Fall, H. Lamers, H. Zinnecker, and S. Glover for valuable discussions, and D. Janies and W. Wheeler for their work on the AMNH Parallel Computing Facility, which we used for the computations presented here. We are grateful to the anonymous referee for useful comments and corrections. YL thanks the AIP for its warm hospitality, and the Kade Foundation for support of her visits there. M-MML acknowledges partial support by NASA ATP grant NAG5-10103, and by NSF CAREER grant AST99-85392. RSK acknowledges support by the Emmy Noether Program of the Deutsche Forschungsgemeinschaft (DFG, KL1358/1).

REFERENCES

- Abel, T, Bryan, G., & Norman, M. L. 2000, ApJ, 540, 39
- Abel, T, Bryan, G., & Norman, M. L. 2002, Science, 295, 93
- Bate, M. R., Bonnell, I. A., & Price, N. M. 1995, MNRAS, 277, 362
- Bate, M. R., & Burkert, A. 1997, MNRAS, 288, 1060
- Benz, W. 1990, in *The Numerical Modeling of Nonlinear Stellar Pulsations*, ed. J. R. Buchler (Dordrecht: Kluwer), 269
- Bonnell, I. & Bastien, P. 1991, ApJ, 374, 610
- Bonnell, I. & Bastien, P. 1993, ApJ, 406, 614
- Bonnell, I. A., Bate, M. R., & Zinnecker, H. 1998, MNRAS, 298, 93
- Bromm, V., Coppi, P. S., & Larson, R. B. 1999, ApJ, 527, L5
- Bromm, V., Coppi, P. S., & Larson, R. B. 2002, ApJ, 564, 23
- Elmegreen, B. G. 1993, ApJ, 419, L29
- Elmegreen, B. G. 2002, ApJ, 577, 206
- Galli, D., Shu, F. H., Laughlin, G., & Lizano, S. 2001, ApJ, 551, 367
- Hartmann, L. 1998, *Accretion Processes in Star Formation* (Cambridge: Cambridge Univ. Press), 33
- Heitsch, F., Mac Low, M.-M. & Klessen, R. S. 2001, ApJ, 547, 280 (Paper III)
- Jeans, J. H. 1902, Phil. Trans.A., 199, 1
- Klessen, R. S. 1997, MNRAS, 292, 11
- Klessen, R. S. 2000, ApJ, 535, 869
- Klessen, R. S. 2001, ApJ, 556, 837 (Paper IV)
- Klessen, R. S., & Burkert, A. 2000, ApJS, 28, 287 (Paper I)
- Klessen, R. S., Burkert, A., & Bate, M. R. 1998, ApJ, 501, L205
- Klessen, R. S., Heitsch, F., & Mac Low, M.-M. 2000, ApJ, 535, 887 (Paper II)

- Kroupa, P. 2002, *Science*, 295, 82
- Lamers, H. J. G. L. M. et al. 2002, *ApJ*, 566, 818
- Low, C., & Lynden-Bell, D. 1976, *MNRAS*, 176, 367
- Mac Low, M.-M., Klessen, R. S., Burkert, A., & Smith, M. D. 1998, *Phys. Rev. Lett.*, 80, 2754
- Mac Low, M.-M. 1999, *ApJ*, 524, 169
- Mac Low, M.-M., & Klessen, R. S. 2003, *Rev. Mod. Phys.*, submitted (astro-ph/0301093)
- Massey, P. 2002, *ApJS*, 141, 81
- Ostriker, E. C., Stone, J. M., & Gammie, C. F. 2001, *ApJ* 546, 980
- Padoan, P., & Nordlund, A. 1999, *ApJ*, 526, 279
- Passot, T., & Vázquez-Semadeni, E. 1998, *Phys. Rev. E*, 58, 4501
- Pudritz, R., 2002, *Science*, 295, 68
- Rouleau, F. & Bastien, P., 1990, *ApJ*, 355, 172
- Salpeter, E. E. 1955, *ApJ*, 121, 161
- Scalo, J. 1998, in ASP Conf. Ser. 142, *The Stellar Initial Mass Function* (38th Herstmonceux Conference), ed. G. Gilmore & D. Howell (San Francisco: ASP), 201
- Smith, M. D., Mac Low, M.-M., & Heitsch, F. 2000, *A&A*, 362, 333
- Spaans, M., & Silk, J. 2000, *ApJ*, 538, 115
- Vázquez-Semadeni, E. & Garcia, N. 2001, *ApJ*, 557, 727
- Vázquez-Semadeni, E., Ballesteros-Paredes, J., & Klessen, R. S. 2003, *ApJ*, in press (astro-ph/0301546)
- Ward-Thompson, D. 2002, *Science*, 295, 76
- Williams, J. P., De Geus, E. J., & Blitz, L. 1994, *ApJ*, 428, 693
- Williams, J. P., Blitz, L., & McKee, C. F. 2000, in *Protostars and Planets IV*, ed. V. Mannings, A. P. Boss, & S. S. Russell (Tucson: Univ. Arizona Press), 97

Yorke, H. W. & Sonnhalter, C. 2002, ApJ, 569, 846

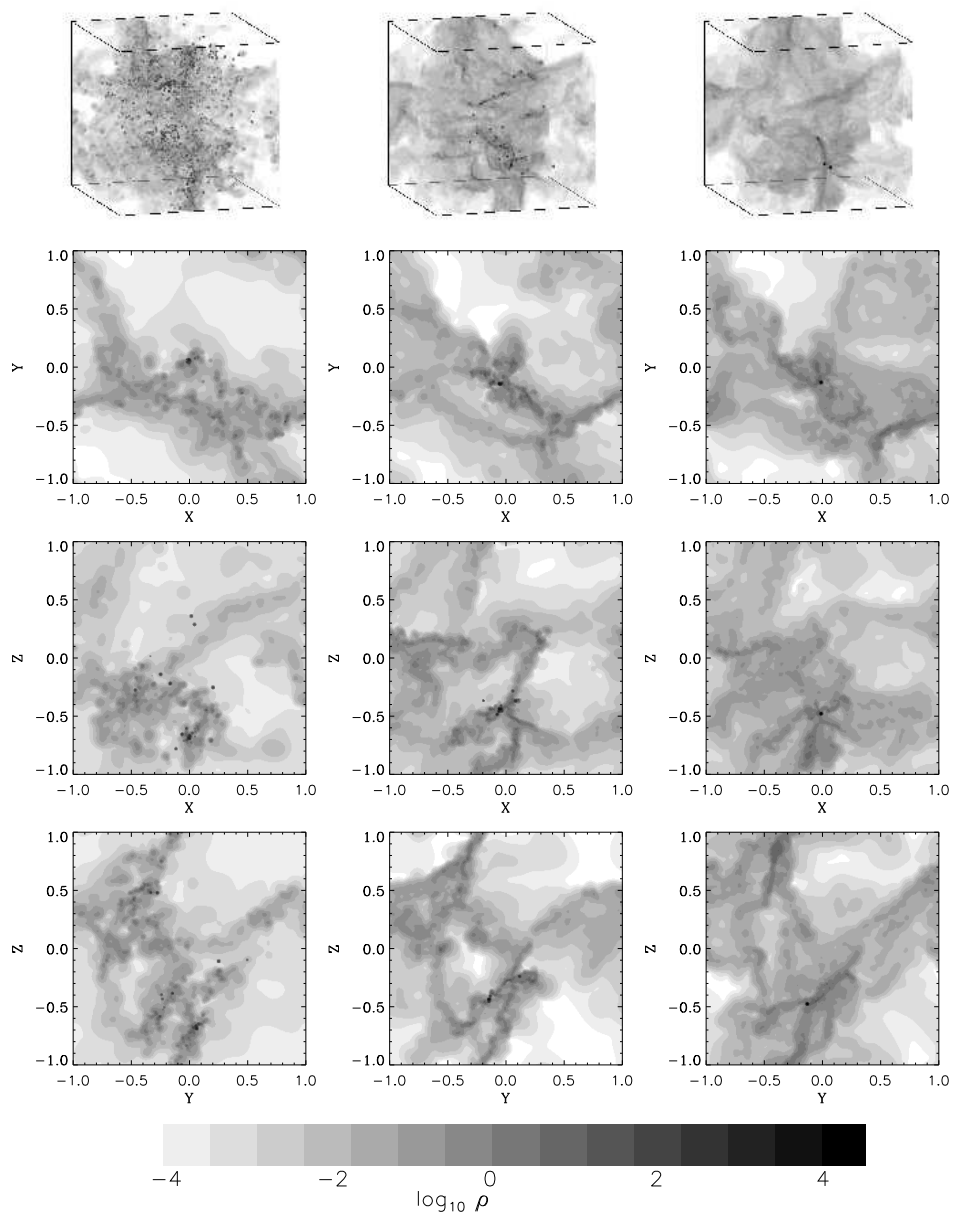


Fig. 1.— Density distribution of the gas shown on a grid in three-dimensional projection (*top row*) and in a slice through maximum density, for driving with $k = 1-2$ at $1 \tau_{ff}$ after self-gravity is turned on. Values of $\gamma = 0.2$ (*left column*), $\gamma = 1.0$ (*middle column*), and $\gamma = 1.3$ (*right column*) are shown. The color bar for the density scale of the slices is at the bottom. Note the very high densities in these images apply to the collapsed cores only. The distribution of gas density is shown in Fig. 7.

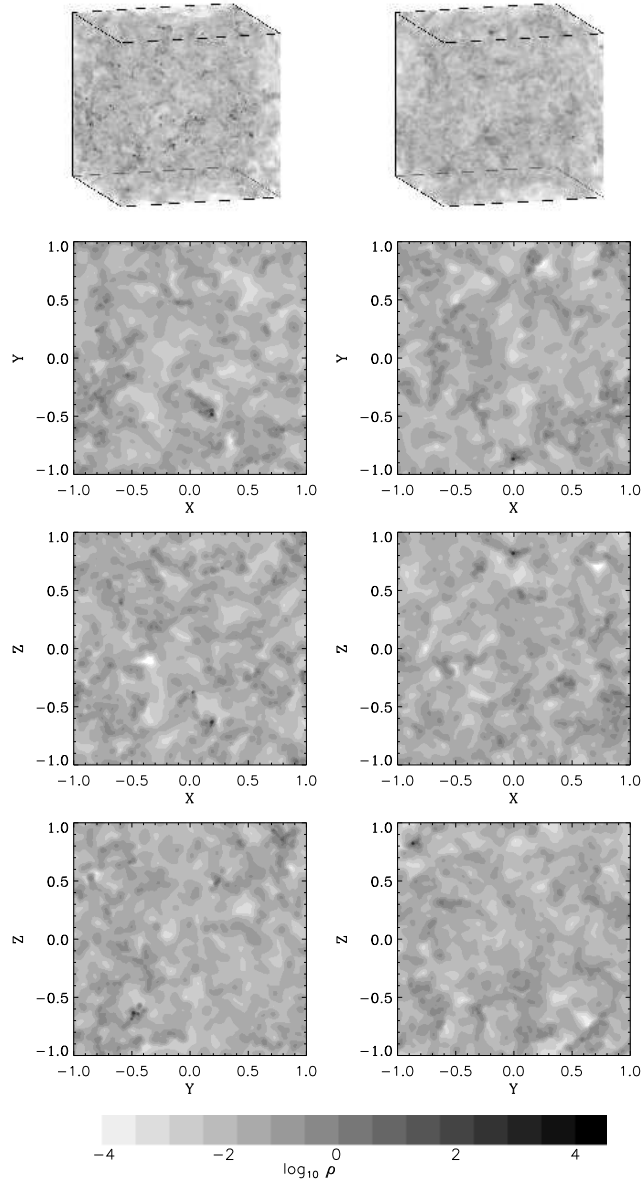


Fig. 2.— Density distribution of the gas shown on a grid in three-dimensional projection (*top row*) and in a slice through maximum density, for selected γ and for driving with $k = 7-8$ at $1 \tau_{ff}$ after self-gravity is turned on. Values of $\gamma = 0.2$ (*left column*), and $\gamma = 1.0$ (*right column*) are shown. The color bar for the density scale of the slices is at the bottom. Note the very high densities in these images apply to the collapsed cores only.

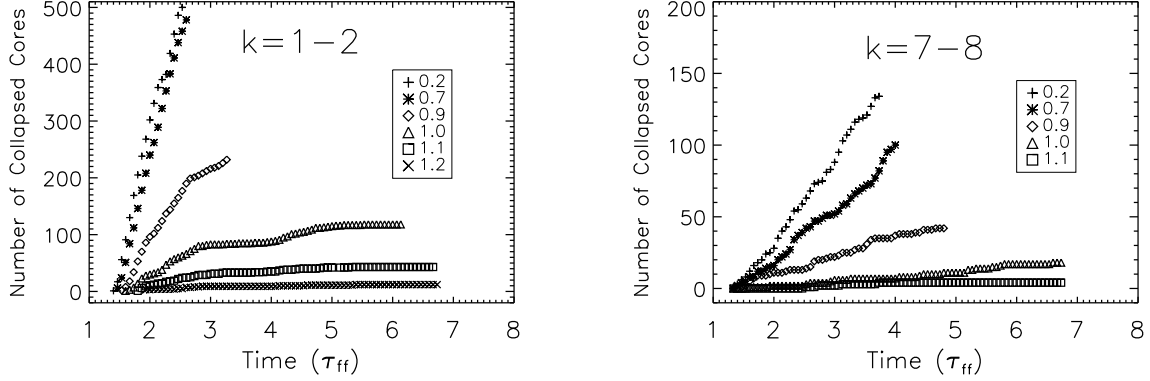


Fig. 3.— Comparison of number of collapsed cores for models with different polytropic exponent γ , for driving with wavenumber $k = 1-2$ (*left panel*) and $k = 7-8$ (*right panel*). Note gravity was “turned on” at $t = 2.0 \simeq 1.33\tau_{ff}$. The simulations of low- γ cases (0.2 and 0.7 in this plot) of model $k = 1-2$ were terminated after a few τ_{ff} due to prohibitively small time step.

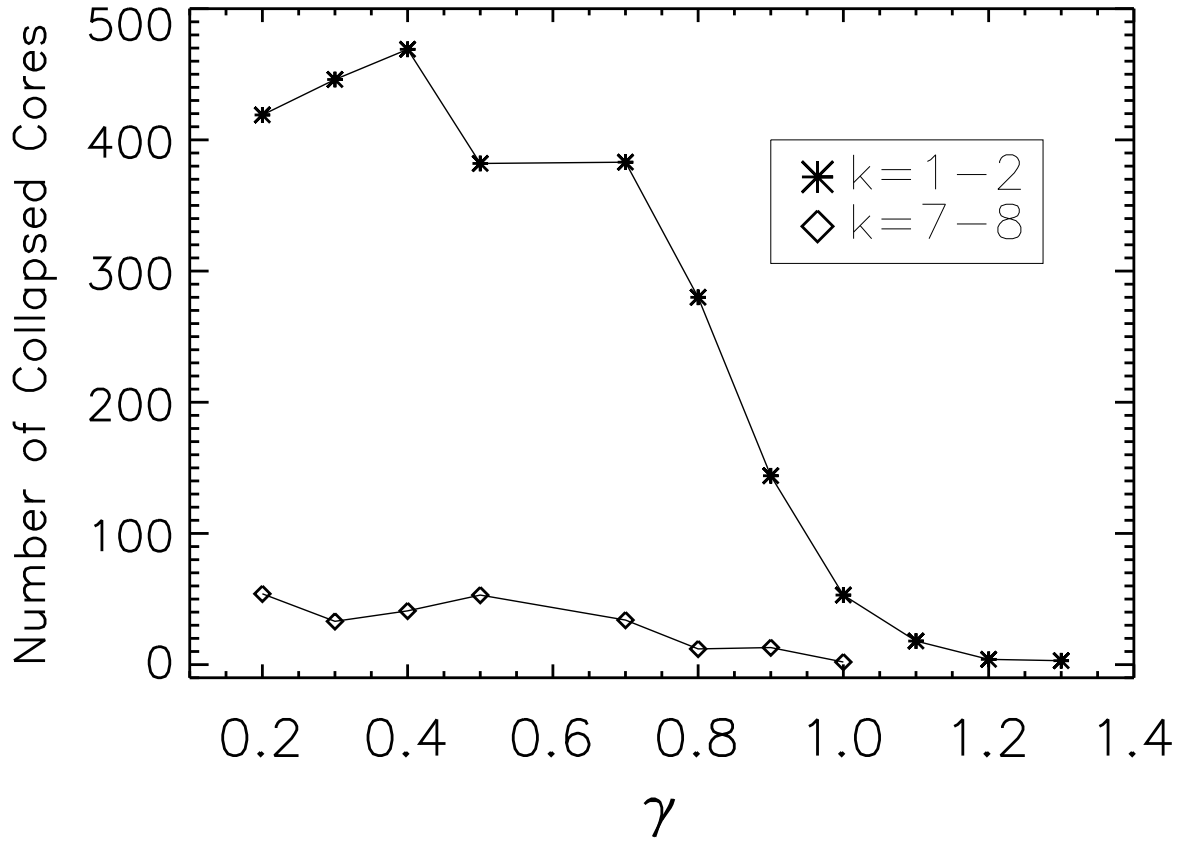


Fig. 4.— Relation of the value of γ to the number of collapsed cores one free-fall time after self-gravity is turned on.

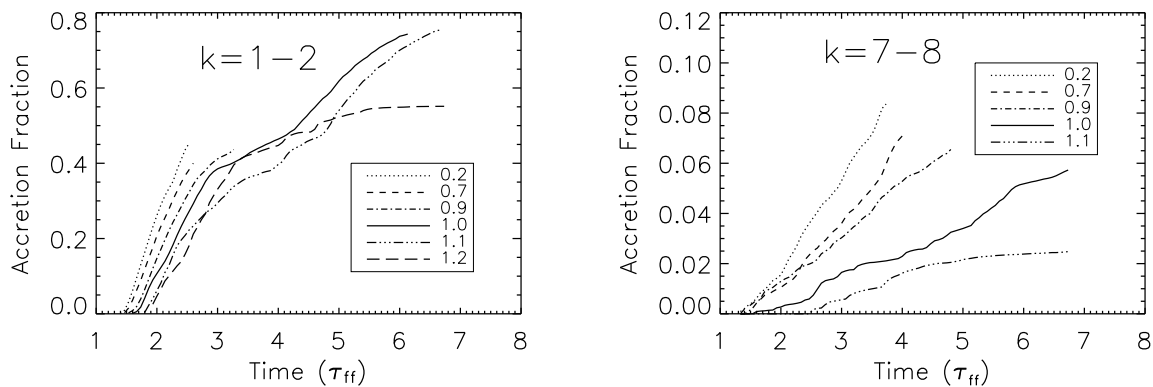


Fig. 5.— Comparison of accretion rate of collapsing cores for turbulence driven with wavenumber $k = 1-2$ (*left panel*) and $k = 7-8$ (*right panel*). Note the different scales in the two plots. Gravity is turned on at $t = 2.0 \simeq 1.33\tau_{ff}$. The simulations of low- γ cases (0.2 and 0.7 in this plot) of the model driven with $k = 1-2$ were terminated after a few τ_{ff} due to the prohibitively small time step.

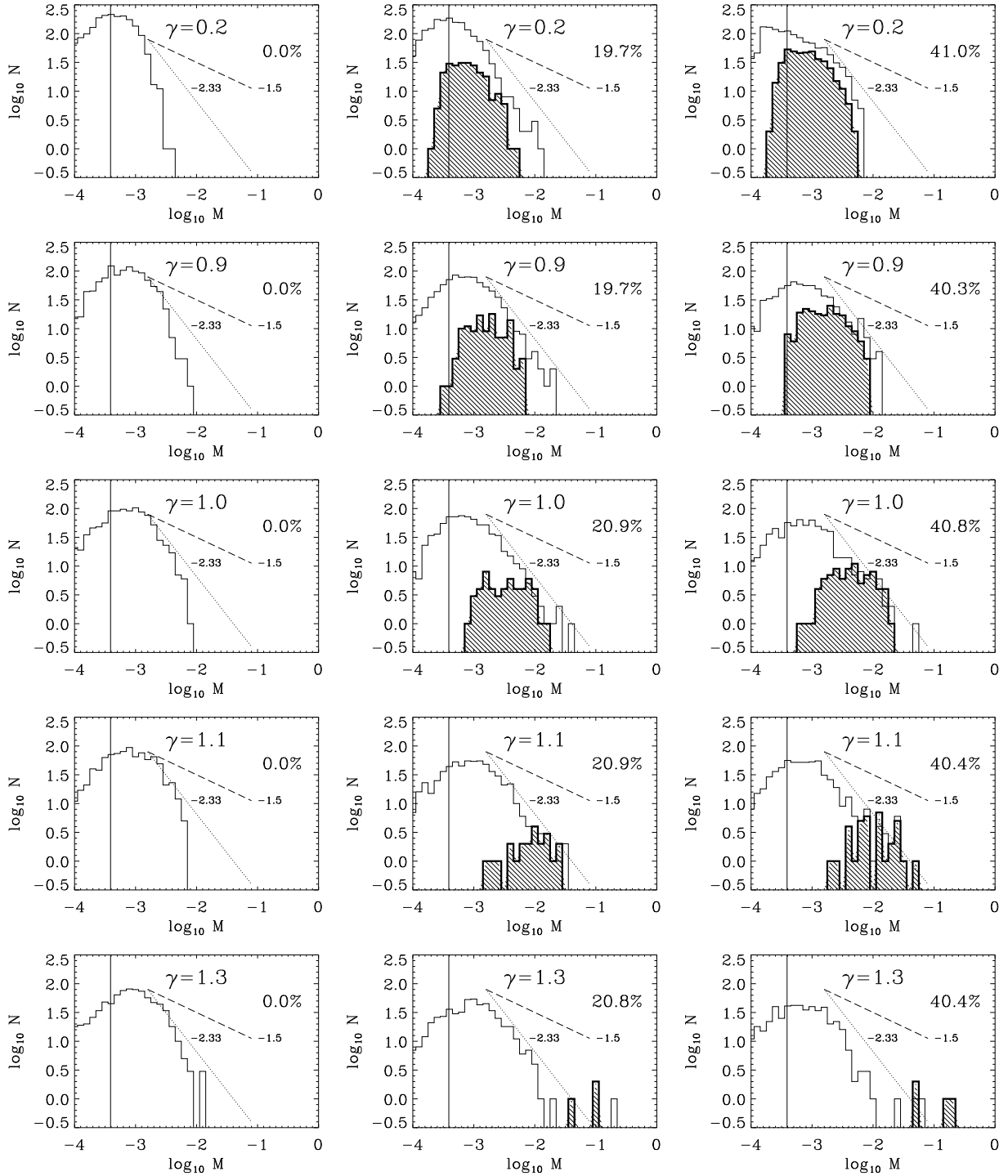


Fig. 6.— Mass spectra of gas clumps (*open histogram*), and of collapsed cores (*filled histogram*) for models with different γ and driving with $k = 1-2$. The fraction of mass accreted into collapsed cores (sink particles) is given for the right two columns. The vertical line shows the SPH resolution limit. Also shown are two power-law spectra with $\nu = -1.5$ (dashed-line) and $\nu = -2.33$ (dotted line).

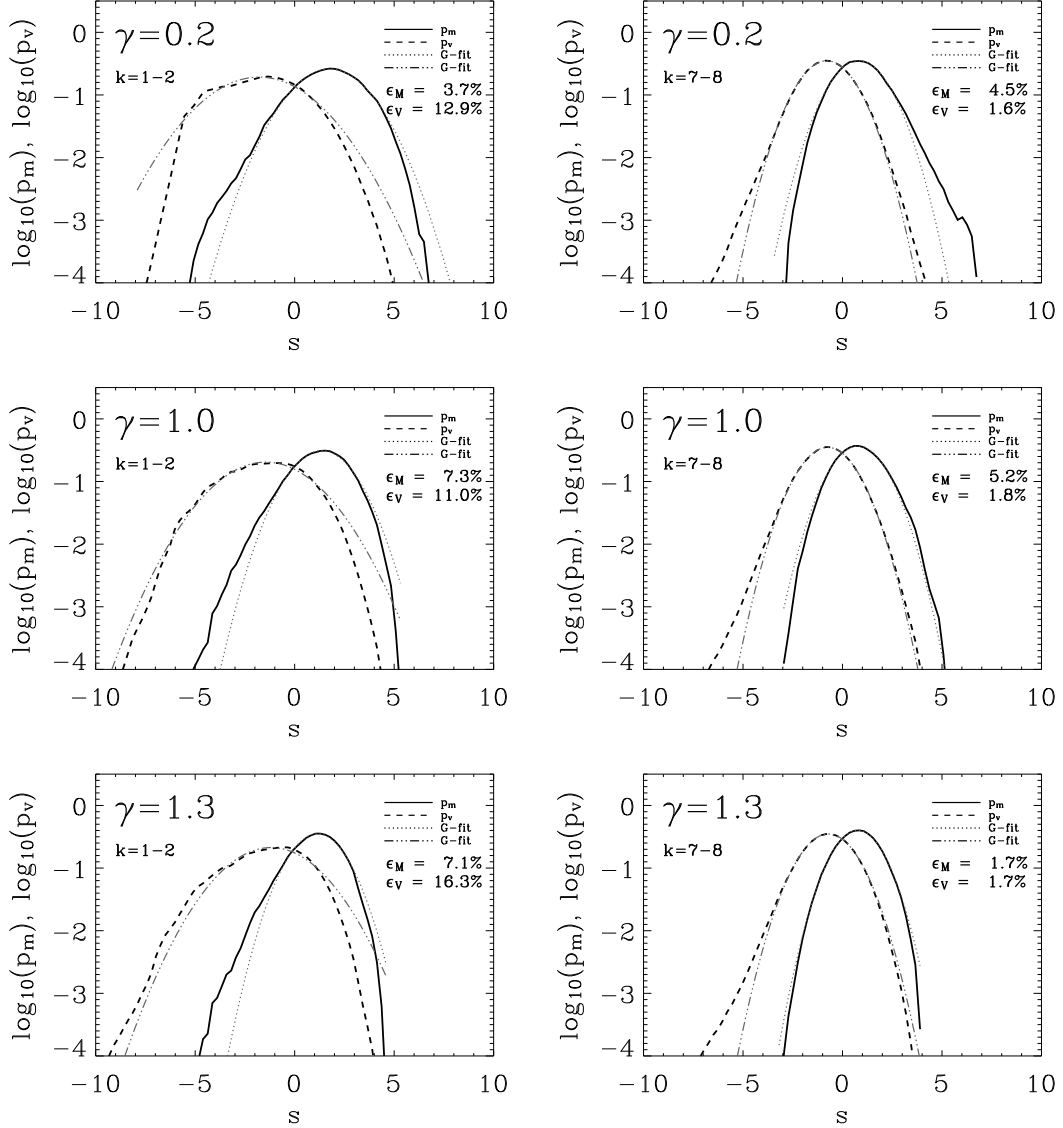


Fig. 7.— Mass-weighted (*thick solid-line*) and volume-weighted (*thick dashed-line*) gas density PDFs p_m and p_v of fully-developed turbulence prior to turning on self-gravity. Models with driving wavenumber $k = 1 - 2$ (*left column*) and $k = 7 - 8$ (*right column*) are shown. Gaussian fits are shown with *thin dotted* and *thin dot-dashed* lines correspondingly, and the errors ϵ_M and ϵ_V summed over the parts of the curves above 10% of the peak values, are quoted. Note that $s = \ln(\rho/\rho_0)$.

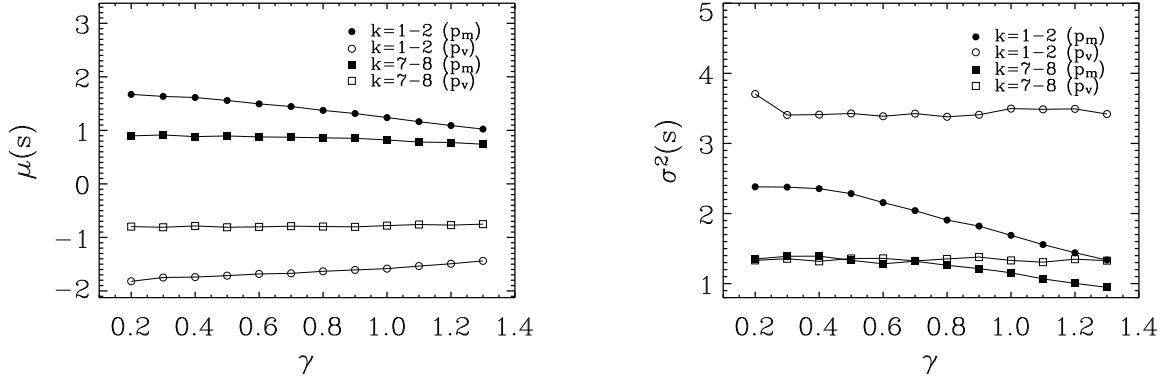


Fig. 8.— First moment (mean) μ (*top*) and second moment (variance) σ^2 (*bottom*), of both p_m (*filled*) and p_v (*open*) as functions of γ , for models driven with wavenumbers $k = 1 - 2$ (*circle*) and $k = 7 - 8$ (*square*), where $s = \ln(\rho/\rho_0)$.

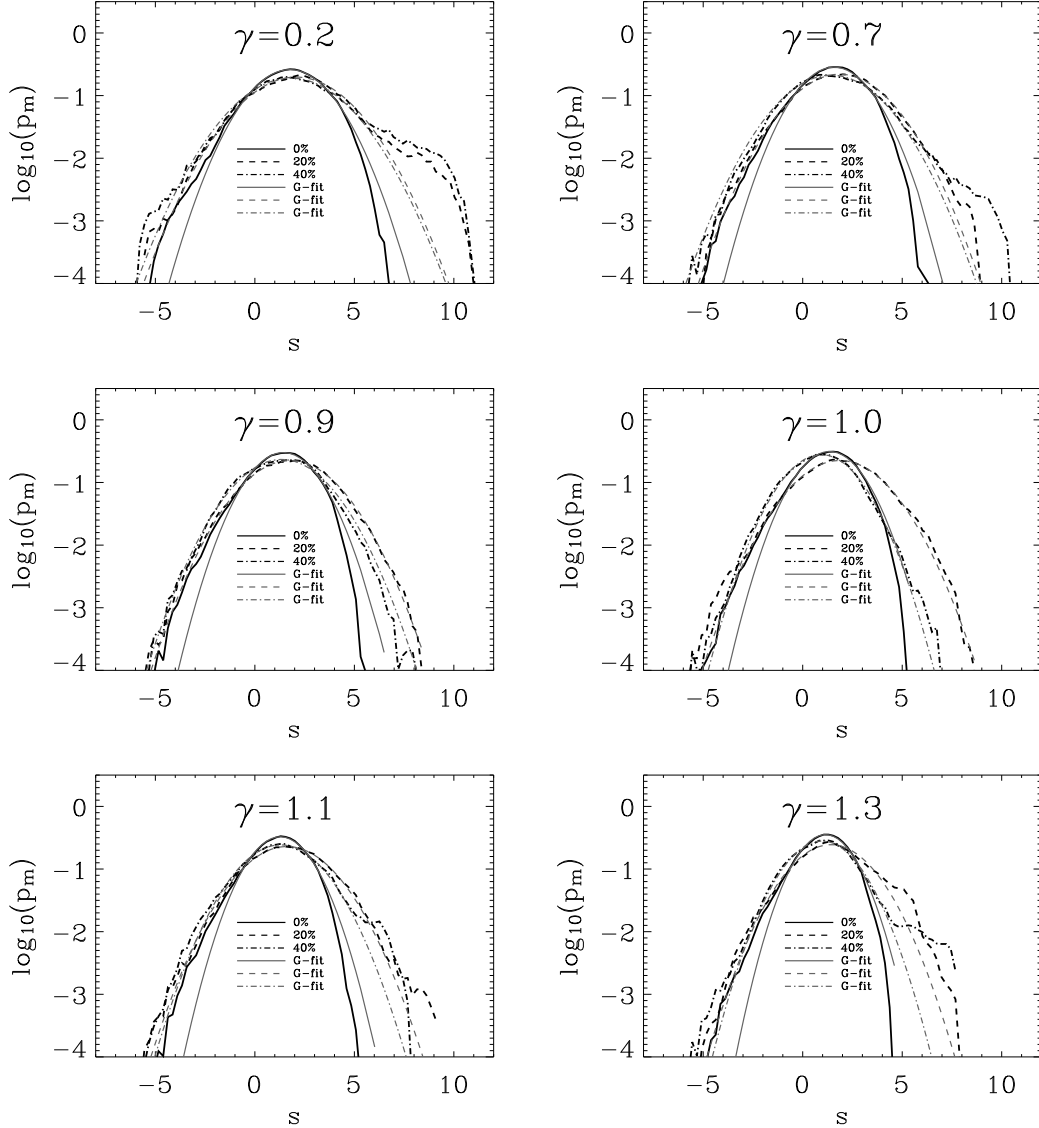


Fig. 9.— Mass-weighted gas density PDFs p_m of models driven with $k = 1 - 2$ for selected γ . Only gas not accreted into sink particles is included. Three evolutionary phases are shown: the initial state (*thick solid-line*), $M_* \approx 20\%$ (*thick dashed-line*), and $M_* \approx 40\%$ (*thick dot-dashed line*). The thin lines (solid, dashed, dot-dashed) are Gaussian fits to the corresponding PDFs above 10% of peak value. Again $s = \ln(\rho/\rho_0)$. Note the change of the high-density tails with γ .

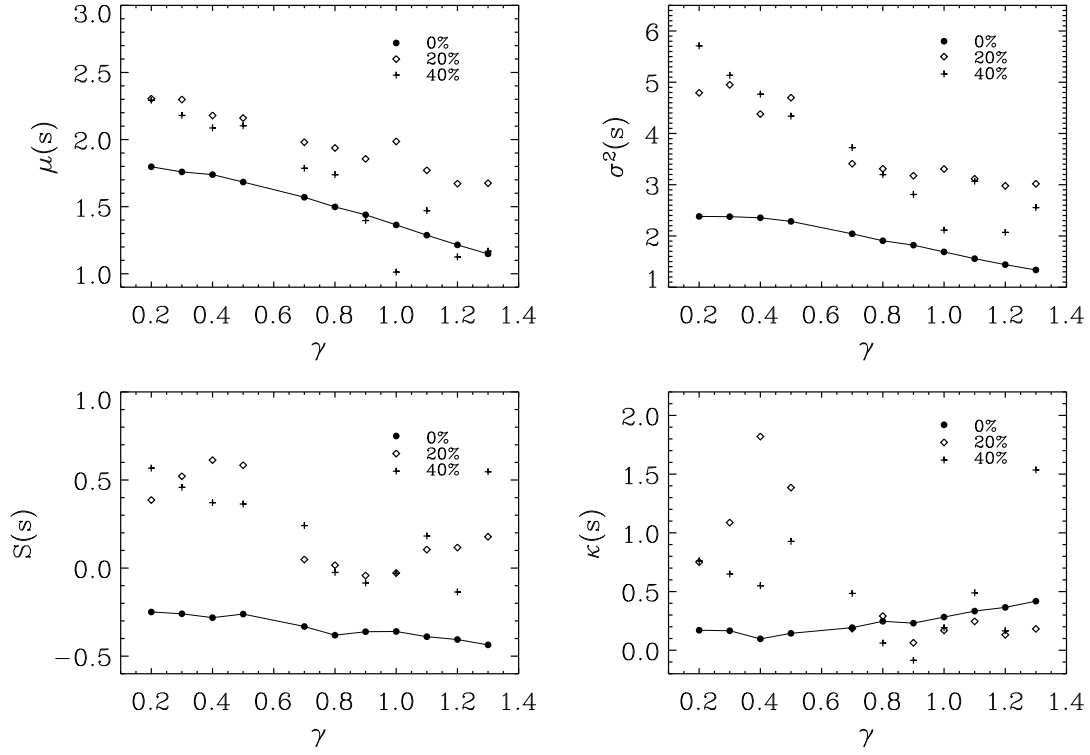


Fig. 10.— The first four moments of three evolutionary phases of the mass-weighted density PDF (corresponding to Figure 9) of the model driven with $k = 1 - 2$, as functions of γ . Shown are the mean μ (top left), variance σ^2 (top right), the skewness S (bottom left), and the kurtosis κ , of $s = \ln(\rho/\rho_0)$. We define the fourth moment κ with a value of 3 subtracted, so that for a Gaussian $\kappa = 0$, while an exponential has $\kappa = 3$.